Received: 19 March 2024 | Revised: 20 September 2024 | Accepted: 10 October 2024

DOI: 10.1002/nbm.5281

RESEARCH ARTICLE

NMR IN BIOMEDICINE WILEY

Paramagnetic salt and agarose recipes for phantoms with desired T1 and T2 values for low-field MRI

Kalina V. Jordanova[1] | Carla C. Fraenza[2] | Michele N. Martin[1] | Ye Tian[3] | Sheng Shen[4] | Christopher E. Vaughn[5,6] | Kevin J. Walsh[7] | Casey Walsh[2] | Charlotte R. Sappo[5,6] | Stephen E. Ogier[1,8] | Megan E. Poorman[9] | Rui P. Teixeira[9] | William A. Grissom[5,6,10] | Krishna S. Nayak[3] | Matthew S. Rosen[4,11] | Andrew G. Webb[12] | Steven G. Greenbaum[2] | Velencia J. Witherspoon[13,14] | Kathryn E. Keenan[1]

[1]Physical Measurement Laboratory, National Institute of Standards and Technology, Boulder, Colorado, USA

[2]Department of Physics and Astronomy, Hunter College, City University of New York, New York, New York, USA

[3]Ming Hsieh Department of Electrical and Computer Engineering, University of Southern California, Los Angeles, California, USA

[4]Athinoula A. Martinos Center for Biomedical Imaging, Massachusetts General Hospital and Harvard Medical School, Boston, Massachusetts, USA

[5]Vanderbilt University Institute of Imaging Science, Vanderbilt University, Nashville, Tennessee, USA

[6]Department of Biomedical Engineering, Vanderbilt University, Nashville, Tennessee, USA

[7]Department of Mechanical and Aerospace Engineering, The Ohio State University, Columbus, Ohio, USA

[8]Department of Physics, University of Colorado Boulder, Boulder, Colorado, USA

[9]Hyperfine, Inc, Guilford, Connecticut, USA

[10]Radiology and Radiological Sciences, Vanderbilt University Medical Center, Nashville, Tennessee, USA

[11]Department of Physics, Harvard University, Cambridge, Massachusetts, USA

[12]C.J. Gorter MRI Center, Department of Radiology, Leiden University Medical Center, Leiden, The Netherlands

[13]Section on Quantitative Imaging and Tissue Sciences, Eunice Kennedy Shriver National Institute of Child Health and Human Development, National Institutes of Health, Bethesda, Maryland, USA

[14]Department of Biomedical Engineering, Tulane University, New Orleans, Louisiana, USA

Correspondence
Kalina V Jordanova, Physical Measurement Laboratory, National Institute of Standards and Technology, 325 Broadway, Boulder CO, 80305 USA.
Email: kalinaj@alumni.stanford.edu

Abstract

Tissue-mimicking reference phantoms are indispensable for the development and optimization of magnetic resonance (MR) measurement sequences. Phantoms have greatest utility when they mimic the MR signals arising from tissue physiology; however, many of the properties underlying these signals, including tissue relaxation characteristics, can vary as a function of magnetic field strength. There has been renewed interest in magnetic resonance imaging (MRI) at field strengths less than 1 T, and phantoms developed for higher field strengths may not be physiologically relevant at these lower fields. This work focuses on developing materials with

Abbreviations: CSF, cerebrospinal fluid; EDTA, editic acid; FFC, fast field cycling; GM, gray matter; MR, magnetic resonance; MRI, magnetic resonance imaging; NMR, nuclear magnetic resonance; PN, part number; qMRI, quantitative MRI; SI, supplemental information; WM, white matter.

Funding information
European Research Council, Grant/Award Number: PASMAR670629; Hyperfine, Inc.; Kiyomi and Ed Baird MGH Research Scholar Award; National Institute of Child Health and Human Development; National Institute of General Medical Sciences, Grant/Award Number: K99GM140338-01; National Institute of Standards and Technology, Grant/Award Number: 70NANB18H006; National Institutes of Health, Grant/Award Numbers: R01 EB032709, R01EB030414; National Research Council; Nederlandse Organisatie voor Wetenschappelijk Onderzoek

specific relaxation properties for lower magnetic field strengths. Specifically, we developed recipes that can be used to create synthetic samples for target nuclear magnetic resonance relaxation values for fields between 0.0065 and 0.55 T. T_1 and T_2 mixing models for agarose-based gels doped with a paramagnetic salt (one of $CuSO_4$, $GdCl_3$, $MnCl_2$, or $NiCl_2$) were created using relaxation measurements of synthetic gel samples at 0.0065, 0.064, and 0.55 T. Measurements were evaluated for variability with respect to measurement repeatability and changing synthesis protocol or laboratory temperature. The mixing models were used to identify formulations of agarose and salt composition to approximately mimic the relaxation times of five neurological tissues (blood, cerebrospinal fluid, fat, gray matter, and white matter) at 0.0065, 0.0475, 0.05, 0.064, and 0.55 T. These mimic sample formulations were measured at each field strength. Of these samples, the $GdCl_3$ and $NiCl_2$ measurements were closest to the target tissue relaxation times. The $GdCl_3$ or $NiCl_2$ mixing model recipes are recommended for creating target relaxation samples below 0.55 T. This work can help development of MRI methods and applications for low-field systems and applications.

KEYWORDS
low-field, neurological, phantoms, quantitative, relaxation

1 | INTRODUCTION

There is renewed interest in magnetic resonance imaging (MRI) at field strengths less than 1 T due to the potential for lower cost, greater portability, quieter operation, improved accessibility, improved implant safety, reduced susceptibility artifacts, and reduced specific absorption rate compared to conventional systems (1.5 and 3 T).[1–3] Many scanners are in development that operate at fields below 1 T.[4–13] Additionally, there are many commercial products available or under development for lower field strengths, including 0.064 T (Swoop, Hyperfine, Guilford, CT, USA), 0.066 T (Promaxo Inc., Oakland CA, USA), 0.345 T (MRIdian Linac, ViewRay, Mountain View, CA, USA), 0.4 T (Magnifico Open, Esaote, Genoa, Italy), 0.5 T (Evry, Synaptive Medical Inc., Toronto, Canada), and 0.55 T (MAGNETOM Free. Max, Siemens Healthineers, Erlangen, Germany).

Tissue-mimicking reference objects (phantoms) are indispensable for developing and optimizing MRI sequences; however, there has been limited development for lower fields. Phantoms help assess the accuracy and generalizability of imaging protocols across scanners and sites[14] and aid in developing and translating quantitative MRI (qMRI) methods to clinical settings.[15] Phantoms have the greatest utility when they mimic the MR signals resulting from tissue physiology. This work focuses on the relaxation properties of phantom materials. Because tissue relaxation properties vary with B_0, phantoms developed with specific relaxation characteristics for > 1 T have relaxation times that do not match tissue relaxation values at low field. Therefore, dedicated effort is needed to develop reference materials for lower fields. Developing a single phantom for all "lower" field instruments is challenging, as it would require the ability to mimic tissue relaxation over a wide range of fields. Therefore, in this work, we provide recipes to target relaxation values using a suite of easily accessible materials, with each recipe applicable to a different field strength.

Specifically, we aimed to create recipes for tissue mimics at 0.0065, 0.064, and 0.55 T. After measuring relaxation properties on a variety of samples that we prepared, we fit mixing models that correlate the concentration of agarose and a chosen paramagnetic salt to T_1 and T_2 at each field strength. While many materials may replicate relaxation properties, we used a mixture of agarose and one of four easily sourced paramagnetic salts ($CuSO_4$, $GdCl_3$, $MnCl_2$, $NiCl_2$). These components are widely available, easy to use, familiar to the MR community,[16–19] and the combination of agarose, and a salt provides two semi-independent levers for modifying T_1 and T_2.[20] We selected agarose rather than agar due to its robustness to bacterial growth and chose to use four salts to offer more options for creating reference samples in a laboratory setting. As a proof of concept, we used the resulting mixing models to create mimics of white matter (WM), gray matter (GM), fat, cerebrospinal fluid (CSF), and blood for each salt at five target field strengths (0.0065, 0.0475, 0.05, 0.064, and 0.55 T) and measured the relaxation values at each field strength.

2 | METHODS

2.1 | T_1 and T_2 mixing models

Mixing models to represent the relationship between either T_1 or T_2 and sample composition were created for mixtures of agarose with one of four salts ($CuSO_4$, $GdCl_3$, $MnCl_2$, $NiCl_2$), for three field strengths (0.0065, 0.064, 0.55 T). For each salt and field, a second-order polynomial model was fit[21,22] relating T_1 and T_2 to salt (N) and agarose (G) concentrations:

$$\frac{1}{T_1} = a_1 + a_2G + a_3G^2 + a_4N + a_5N^2 + a_6GN + a_7G^2N + a_8GN^2 + a_9G^2N^2 \quad (1)$$

$$\frac{1}{T_2} = b_1 + b_2G + b_3G^2 + b_4N + b_5N^2 + b_6GN + b_7G^2N + b_8GN^2 + b_9G^2N^2 \quad (2)$$

These models were fit using T_1 and T_2 times measured from a set of test samples at each field strength (sample protocol and measurement details below). Deionized water measurements established $\{a,b\}_1$. Then, an agarose-only model limited to the first three terms was fit to determine $\{a,b\}_{2-3}$. A salt-only model was fit to determine $\{a,b\}_{4-5}$. Finally, $\{a,b\}_{1-5}$ were fixed when modeling Equations 1–2 with all terms. Coefficients were constrained to be nonnegative, and small coefficients below 1×10^{-4} were set to zero (no appreciable effect was observed in the fit).

To use the mixing models as recipes for creating mimic samples, agarose and salt concentrations can be calculated for target T_1 and T_2 times by inverting Equations 1–2 using Python `sympy` for each field strength. For this study, mimic sample compositions were calculated for five field strengths (0.0065, 0.0475, 0.05, 0.064, and 0.55 T), wherein for the 0.0475 and 0.05 T samples, the 0.064 T mixing models were used as a proxy for the models at those field strengths.

2.2 | Sample preparation protocols

To obtain data to fit the mixing models, test samples of mixtures of agarose and a salt (Millipore-Sigma, St. Louis, MO, USA) were identified to span a wide range of T_1 and T_2, and their relaxation properties were measured. Sample materials were chosen to be readily available and to minimize toxicity. They included $CuSO_4{\cdot}5H_20$ (part number [PN]: 209198), $GdCl_3{\cdot}6H_20$ (PN: 203289), edetic acid (EDTA) (PN: 324503), $MnCl_2{\cdot}4H_20$ (PN: 221279), $NiCl_2{\cdot}6H_20$ (PN: N6136), and agarose (PN: A6013).

Test samples were prepared by dissolving stock solutions of salt compounds in deionized water. The $GdCl_3$-EDTA stock solution was made by stirring $GdCl_3$ and EDTA at a 1:2 molar ratio at 98°C for 30 min. Agarose was added to the salt solution for samples requiring a gelling agent. The solution underwent two heat cycles comprising a 30-s interval microwave cycle until boiling and a 10-min hotplate cycle to ensure well-hydrated agarose.[16] Partway through the study, this protocol was adjusted to account for evaporative loss, and additional deionized water was added to the agarose following the heat cycles. The revised protocol was used for 18 of 45 agarose test samples. The remaining agarose samples, as well as the salt-only samples, omitted evaporative loss correction. The final mixtures were poured into vials (50 mL, 30 mL, or 10 mm nuclear magnetic resonance [NMR] tubes) pre-rinsed with isopropyl alcohol to minimize bubble formation. Samples were prepared in large batches and divided into multiple individual vials, which were each subsequently shipped to different measurement sites (see below for measurement site details). Test sample compositions are listed in Table S1.

2.3 | T_1 and T_2 measurement

Mixing models were created for each salt by fitting the models to measured sample data at 0.0065, 0.064, and 0.55 T. This work was part of a multi-institutional effort; thus, measurements for each field strength were conducted on a different system at a different site. At 0.0065 T, measurements were made on an ultra-low-field scanner.[5,23] At 0.064 T, measurements were made on a Hyperfine Swoop (hardware 1.8, software rc8.5.0 and rc8.6.0, Guilford, CT, USA). At 0.55 T, measurements were made on a prototype MAGNETOM Aera XQ (Siemens Healthineers, Erlangen, Germany).

Additional measurements were acquired to validate and analyze measurement accuracy. Supplemental temperature-controlled measurements were acquired on two variable field NMR systems: the first magnet (Resonance Research Inc. BFM-0C, Billerica, MA, USA) was set to 0.0065 T, and the second magnet (Bruker B-E25, Billerica, MA, USA) was set to either 0.064 or 0.55 T.

Finally, access to a fast field cycling (FFC) relaxometer (Spinmaster FFC2000 1T Relaxometer, Stelar s.r.l., Mede [PV], Italy) allowed for additional T_1 measurements to be made over a range of field strengths using only one system to compare relaxation dispersion trends for different salt and agarose mixtures.

Although the measurement protocols were not enforced to be the same between sites, all sites used a form of an inversion-recovery sequence to measure T_1 and a spin-echo sequence to measure T_2. Additional details for each measurement system, as well as the measurement protocols, are listed in Table S2.

2.4 | T_1 and T_2 measurement evaluation metrics

Because the measurements made for this study were multi-institutional and made on different systems, some variability in relaxation measurement is expected. To understand the magnitude of the measurement variability, relaxation time measurements were assessed for three conditions: (1) variation in *repeat* measurements made on different measurement days that were 20 days apart, (2) variation in measurements for samples made using each preparation *protocol* (with and without evaporative loss correction), and (3) variation in measurements made at different *temperatures*. Due to scan time and sample preparation limitations, not all samples could be measured for each variability condition. Specifically, *repeat* measurements were made for 15 samples at 0.55 T. *Sample-preparation protocol*-dependent measurements were made for seven samples that were prepared in duplicate using different protocols at 0.0065, 0.064, and 0.55 T. *Temperature*-dependent measurements were made for 49 samples for 0.0065 T, for 10 of the 49 samples for 0.064 T, and for 16 of the 49 samples for 0.55 T. Note that temperature was not controlled in the *sample-preparation protocol* dependence or *repeatability* measurements. To assess variability, measurements were normalized to the mean measurement for each sample, and the mean, minimum, and maximum variations were noted for each condition. Variability within ±10% of the mean measurement value was deemed to be acceptable. Note that to fit Equations 1–2, test sample measurements were limited to those that were closest to the target temperature of 20°C for each field strength. If multiple samples were measured at the same temperature and field strength, the average of their measurements was used in the mixing model fitting process.

2.5 | Proof of concept: tissue mimics using mixing model recipes

To demonstrate the mixing models' application to producing tissue mimics, five tissues were selected for creating T_1 and T_2 sample mimics: blood, CSF, fat, GM, and WM. Literature data supplemented with T_1 ex vivo FFC measurements were used to identify target T_1 and T_2 relaxation times for each tissue at five field strengths. This involved fitting relaxation dispersion models to tissue-specific relaxation data and interpolating the target values at the relevant field strengths. Details about the data and dispersion models can be found in Figures S1–S2 and Tables S3–S4.

Once target relaxation times were identified for each tissue, each salt's mixing model was used to calculate agarose and salt concentrations that could serve as a mimic for the target T_1 and T_2. Because the agarose concentrations for the CSF mimics were very small, which can be difficult to synthesize, deionized water was included as an additional potential CSF mimic. For targets lying entirely outside the T_1-T_2 sample space, mimic samples were calculated to target T_1 or T_2 separately.

Mimic samples were created using the evaporative-corrected protocol described previously, and relaxation times were measured for five fields of interest. These measurements were made using the systems described above for the three mixing model field strengths (0.0065, 0.064, and 0.55 T), and for two additional field strengths using two different systems (0.0475 and 0.05 T). At 0.0475 T, the measurement system was a Sigwa open bi-planar permanent magnet (Sigwa MRI, Boston, MA, USA). At 0.05 T, the system was a point-of-care permanent magnet-based Halbach array.[24] For 0.0475 and 0.05 T, the mimic sample compositions were calculated using the 0.064 T mixing models. These additional field measurements allowed for the assessment of how accurately mimics can be made from the mixing models when the target is at a slightly different field strength.

The percent error was calculated between the measured and target T_1 and T_2 for each tissue, salt, and field. This was used to evaluate how accurately the mimics represented tissue relaxation properties with the minimum, maximum, and average absolute errors reported for each salt and field.

3 | RESULTS

3.1 | T_1 and T_2 mixing models

Results of the fitted coefficients for the mixing models (Equations 1–2) for 0.0065, 0.064, and 0.55 T are given in Tables 1–4. The higher order coefficients tended toward zero at 0.0065 T for all salts except $MnCl_2$. For $MnCl_2$, the higher order coefficients were largest for the 0.0065 T model. Relaxation measurement results for each sample used in fitting the mixing models are shown in Figures S3–S6.

TABLE 1 $CuSO_4$ and agarose mixing model coefficients for models fit to 0.0065, 0.064, and 0.55 T T_1 and T_2 measurements.

	0.0065 T		0.064 T		0.55 T	
Coeff #	T_1 (a)	T_2 (b)	T_1 (a)	T_2 (b)	T_1 (a)	T_2 (b)
1	0.428	0.65	0.412	0.462	0.391	0.454
2	1.07	7.68	0.158	7.03	0.0324	7.47
3	0	0.0366	0.0185	0	0.00651	0.986
4	1.71	1.76	1.52	1.52	0.703	0.703
5	0.23	0.194	0.262	0.262	0.144	0.144
6	1.25	1.75	0.83	2.88	0.239	0
7	0	0	0	0	0.0182	0.146
8	0	0	0	0	0.000123	0
9	0	0	0	0	0.0212	0.98

TABLE 2 $GdCl_3$-EDTA and agarose mixing model coefficients for models fit to 0.0065, 0.064, and 0.55 T T_1 and T_2 measurements.

	0.0065 T		0.064 T		0.55 T	
Coeff #	T_1 (a)	T_2 (b)	T_1 (a)	T_2 (b)	T_1 (a)	T_2 (b)
1	0.428	0.65	0.412	0.462	0.391	0.454
2	1.07	7.68	0.158	7.03	0.0324	7.47
3	0	0.0366	0.0185	0	0.00651	0.986
4	18.3	18.3	15.6	15.6	8.5	8.5
5	0	0	0	0	0	0
6	0	0.0188	0	7.56	0	16.2
7	0	0	0	0.00658	0	0
8	0	7.84	0	0	0	0
9	0	0	0	0	0	0

TABLE 3 $MnCl_2$ and agarose mixing model coefficients for models fit to 0.0065, 0.064, and 0.55 T T_1 and T_2 measurements.

	0.0065 T		0.064 T		0.55 T	
Coeff #	T_1 (a)	T_2 (b)	T_1 (a)	T_2 (b)	T_1 (a)	T_2 (b)
1	0.428	0.65	0.412	0.462	0.391	0.454
2	1.07	7.68	0.158	7.03	0.0324	7.47
3	0	0.0366	0.0185	0	0.00651	0.986
4	27.6	42.7	18.1	34.2	8.59	42.5
5	0	0	0	0	0.188	0
6	1	1	0	0	2.96	4.96
7	1	1	0	0	0.0183	0
8	1	1	0	0	0	0.125
9	1	1	0	0	0	0

3.2 | T_1 and T_2 measurement evaluation metrics

T_1 and T_2 measurements were measured at multiple institutions using different NMR or MRI systems at different ambient temperatures over 1.5 years, and with samples made from different sample protocols. To understand the uncertainty in these measurements, the variation in measured relaxation times under different conditions (*repeatability*, *sample-preparation protocol* dependence, and *temperature* dependence) was assessed at 0.0065, 0.064, and 0.55 T. See the Figures S7–S13 for variation data presented in plot format.

TABLE 4 $NiCl_2$ and agarose mixing model coefficients for models fit to 0.0065, 0.064, and 0.55 T T_1 and T_2 measurements.

	0.0065 T		0.064 T		0.55 T	
Coeff #	T_1 (a)	T_2 (b)	T_1 (a)	T_2 (b)	T_1 (a)	T_2 (b)
1	0.428	0.65	0.412	0.462	0.391	0.454
2	1.07	7.68	0.158	7.03	0.0324	7.47
3	0	0.0366	0.0185	0	0.00651	0.986
4	0.549	0.624	0.568	0.568	0.652	0.652
5	0.00112	0.000948	0	0	0.000977	0.000977
6	0	0.0739	0	0	0	0
7	0	0	0	0	0	0
8	0	0	0	0.00504	0	0.0525
9	0	0.0372	0	0	0	0

TABLE 5 Summary statistics of the mean absolute normalized error, as well as the minimum and maximum normalized error seen for any sample, for all variability conditions and field strengths. Specifically, variation due to measurement *repeatability*, *protocol* dependence, and *temperature* dependence were evaluated on a subset of samples for a subset of field strengths. Dashes indicate that the condition was not evaluated for that field strength. Conditions with normalized error above 10% are bolded, namely, for the minimum and maximum error ranges for 0.064 and 0.55 T *protocol* dependence and for 0.0065 T *temperature* dependence.

		Field (T)					
		0.0065	0.064	0.55	0.0065	0.064	0.55
		Mean absolute normalized error (%)			Minimum and maximum sample normalized error (%) (number of samples with absolute error above 10%)		
T_1	Repeatability	-	-	1.1	-	-	±1.9 (0/15)
	Protocol dependence	4.7	7.2	5.9	±5.6 (0/2)	**±17.8 (1/7)**	**−14.4 to 15.5 (1/4)**
	Temperature dependence	4.2	2.9	1.7	−9.9 to 9.0 (0/49)	−6.7 to 6.5 (0/10)	−6.9 to 6.6 (0/27)
T_2	Repeatability	-	-	1.7	-	-	±3.8 (0/15)
	Protocol dependence	5.6	4.8	9.2	±6.5 (0/2)	±8.0 (0/7)	**−14.1 to 14.3 (4/4)**
	Temperature dependence	4.3	1.3	1.4	**−19.3 to 11.3 (3/49)**	±4.1 (0/10)	−5.8 to 5.3 (0/27)

Table 5 shows summary statistics of the mean absolute normalized error, as well as the minimum and maximum normalized error for any sample at all conditions and field strengths. For all conditions and field strengths, the mean absolute normalized error was less than 10%, indicating the variation is within the limits of acceptability, ±10%.

For some conditions and field strengths, the minimum and maximum normalized errors seen for a sample exceeded 10%. The number of samples with a minimum or maximum normalized error greater than 10% are indicated in Table 5. In general, very few samples had error above 10%, except for the *sample-preparation protocol*-dependent 0.55 T measurements for which all four samples had error larger than 10%. Note that even for this condition, the minimum and maximum normalized error was less than 15%, and many of these errors were approximately 10%. Overall, 98.2% of the T_1 measurements and 93.9% of the T_2 measurements had minimum and maximum absolute errors less than 10%.

3.3 | Proof of concept: tissue mimics using mixing model recipes

Mimic samples for five tissues were created for each field strength and each salt composition. Results comparing the measured T_1 and T_2 for each mimic to its target T_1 and T_2 for the $NiCl_2$ samples are shown in Figure 1 (see the Figures S14–S16 for results for other salts).

Accuracy was examined by calculating the error of each mimic's measured T_1 and T_2 from the target T_1 and T_2. The mimic sample compositions, target and measured T_1 and T_2, and mimic relaxation errors are given in Tables S5-S8. Figure 2 shows mimic relaxation errors for T_1 and T_2, for each salt and field. Note that the $NiCl_2$ errors in Figure 2 correspond to the measurements plotted in Figure 1. For all CSF mimics and for the $MnCl_2$ formulated fat mimics, the relaxation error is high, because the tissue relaxation times were outside of the range of the mixing

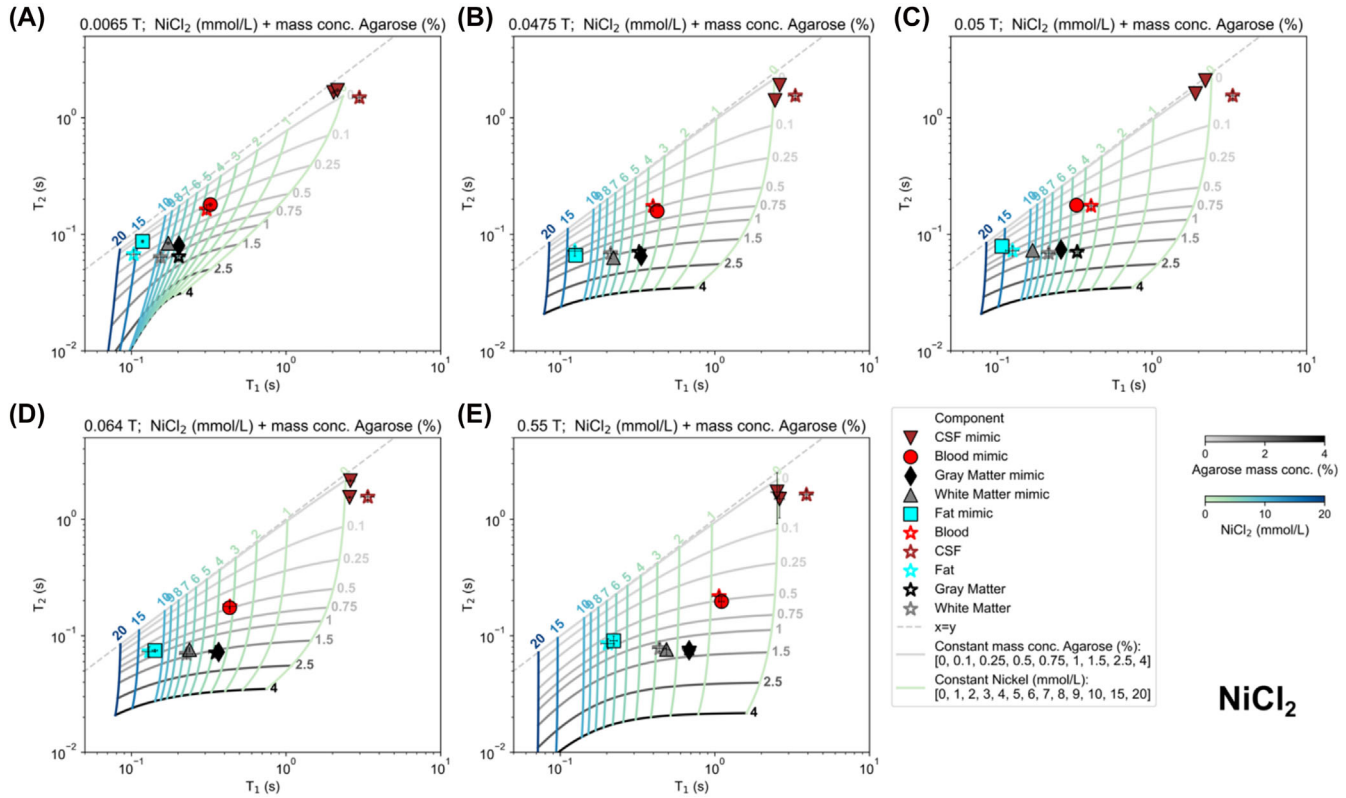

FIGURE 1 T_1 and T_2 mimic sample measurements and mixing models for $NiCl_2$ with agarose for (A) 0.0065 T, (B) 0.0475 T, (C) 0.05 T, (D) 0.064 T, and (E) 0.55 T. Target tissue T_1 and T_2 times (stars; blood = red, CSF = maroon, fat = blue, GM = black, WM = gray) are shown. Each mimic measurement is shown with the same color as its tissue, and twice the standard deviation is plotted as error bars. Mixing models are displayed via constant agarose concentration lines (gray) and constant $NiCl_2$ concentration lines (blue-green). Dashed gray line represents $T_1 = T_2$.

model concentration limits. Excluding CSF, which could not be mimicked by any salt, the percentages of mimics with less than 10% relaxation error (the counts of data points within the 10% confidence interval) were 35.0%, 62.5%, 42.9%, and 72.5% for $CuSO_4$, $GdCl_3$-EDTA, $MnCl_2$, and $NiCl_2$, respectively. $NiCl_2$ samples exhibited less than 10% error for the largest number of samples.

Finally, the T_1 of WM and GM mimics was measured on the FFC system across field strengths. Figure 3 shows T_1 measurements of the WM and GM mimics made on the FFC, as well as the WM and GM relaxation dispersion models (see the Table S4 for dispersion model details). Some of the $GdCl_3$-EDTA FFC measurements remained close to the dispersion models for a large field range: for example, the 0.0064 T mimic for WM stays within 10% of the WM T_1 targets between 0.0035 and 0.43 T, indicating that it could serve as a WM T_1 mimic for that entire field range.

4 | DISCUSSION AND CONCLUSION

Models for mixtures of agarose and one of four paramagnetic salts were created that can be used to determine recipes for tissue mimics at low MRI field strengths of 0.0065, 0.064, and 0.55 T. T_1 and T_2 measurements for a total of 138 unique samples (52 unique test samples and 86 unique mimic samples) were measured at six institutions using eight different NMR or MRI systems at different ambient temperatures over 1.5 years. These measurements were used to create and validate the mixing models.

4.1 | T_1 and T_2 mixing models

T_1 and T_2 mixing models were fit for four salt and agarose mixtures, for three fields of interest. The constraints for the coefficients of the polynomial mixing models were empirically chosen to be 0 or greater than 1×10^{-4} for all coefficients in this study; however, future work that defines these constraints on a per-coefficient basis could improve the resulting mixing model fits to the measured data. Furthermore, the mixing models are sensitive to the accuracy of the measured T_1 and T_2 for each test sample. Known sources of measurement variation include variable

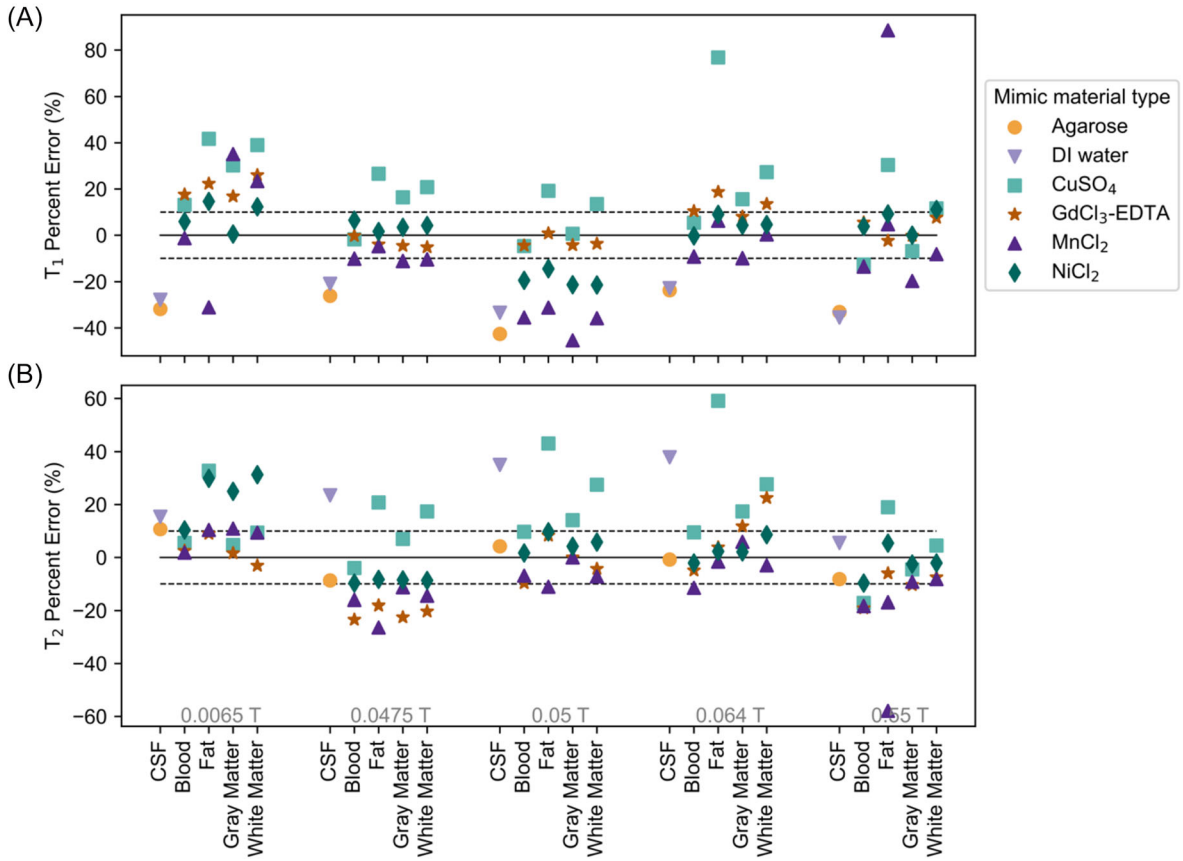

FIGURE 2 (A) T_1 and (B) T_2 mimic sample measurement error compared to the target T_1 and T_2 times, as a function of field strength, tissue, and mimic material type. Note that the $NiCl_2$ errors correspond to the measurements plotted in Figure 1.

laboratory temperature, variations in sample synthesis protocols, and variations that come from the measurement sequence parameters and fitting routines of the individual measurement sites. To minimize the variations between sites, the measurement protocols all used inversion-recovery or spin-echo techniques to measure T_1 and T_2, respectively. However, the fitting routines were not consistent across all sites; for some systems, the team did not have access to the raw data, only the resulting quantitative map. A potential improvement to this study would be centralized data processing. To assess the impact on relaxation measurements due to the other sources, measurement variation was analyzed via repeated measurements over time, changes in sample-preparation protocols, and variations in temperature. In general, variations in measurement were within ±10% of the measurement average. The repeat measurement variation can assess whether homogenization of the oxygen concentration occurred prior to the first measurement. The samples with repeat measurements had a mean error of less than 1.7%, with a maximum error of 3.8% for any sample (see Table 5), indicating there was sufficient time for homogenization of the samples. We note that using the same temperatures and sample protocol for all measurements could improve this study. However, as presented here, this study better replicates the expected use of the mimics, which will likely be used in various laboratory conditions by the community.

We recommend that after a sample is made using one of the recipes determined in this study, their T_1 and T_2 times are carefully measured using validated measurement methods to give reference values, before using the samples for other development and testing. These materials can be used in any format, including anthropomorphic shapes.[25–30] The dependence of relaxation times on temperature is known for many of the salts used in this study[19,31–33]; thus, we recommend that temperatures be recorded for both reference measurements and test measurements of any prepared samples. Finally, relaxation properties should be measured periodically, as sample relaxation properties can change over time. Extensive stability measurements over time were outside the scope of this study; however, studies have shown stability of salt and agarose mixtures of up to 350 days.[17]

4.2 | Proof of concept: tissue mimics using mixing model recipes

Sample compositions for four salt and agarose mixtures were determined for 0.0065, 0.0475, 0.05, 0.064, and 0.55 T that are suitable as T_1 and T_2 tissue mimics at laboratory temperatures of approximately 20°C for blood, CSF, fat, GM, and WM. A repository that provides the functionality

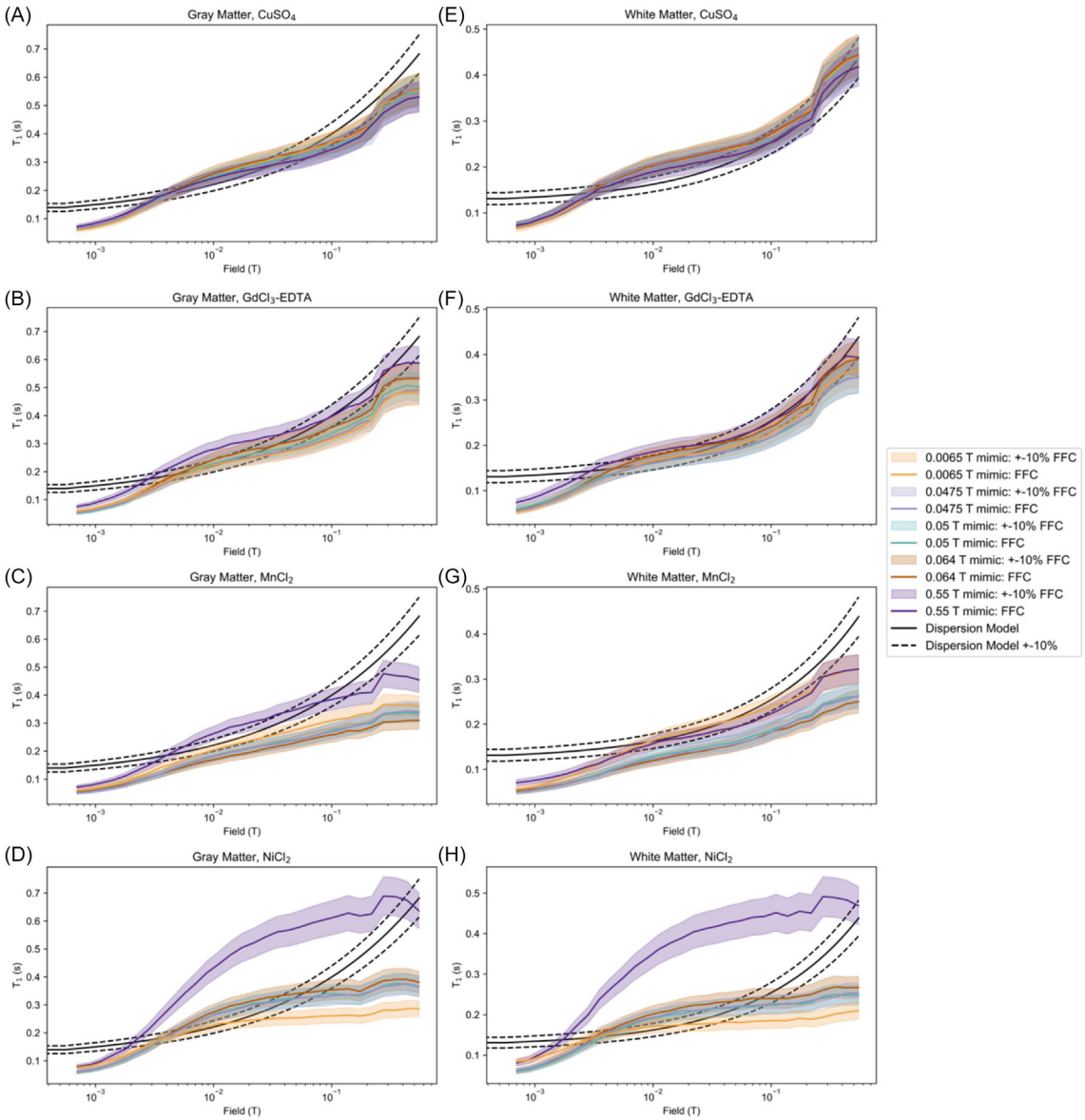

FIGURE 3 (A–D) GM and (E–H) WM mimic sample T_1 dispersion data measured on an FFC system (colored lines), along with a 10% variation of the measurements (shaded colored regions) for (A, E) $CuSO_4$, (B, F) $GdCl_3$-EDTA, (C, G) $MnCl_2$, and (D, H) $NiCl_2$. Mimics are labeled by their target field. The T_1 dispersion model that produced the field-specific targets for each tissue are plotted (black lines). EDTA, editic acid; FFC, fast field cycling; GM, gray matter; WM, white matter.

to solve for tissue mimic compositions given target tissue relaxation times for a particular field strength has been made available online at https://github.com/usnistgov/mri-tissue-mimics.

Mimic sample relaxation times were compared to respective target relaxation times. Differences between measured and target relaxation can be due to several factors, including sample preparation techniques, systematic measurement error, and errors that propagate from the mixing models themselves when computing sample concentrations. The $NiCl_2$ mimic sample measurements had the lowest magnitude of percent error compared to their target values, and $GdCl_3$-EDTA measurements were second lowest. Note that $NiCl_2$ has relatively low relaxivity, and therefore, those samples are less susceptible to errors when weighing the $NiCl_2$ to prepare the stock solutions. All salts failed to mimic the relaxation values of CSF due to the difference between lab temperatures (approximately 20°C) and body temperature (approximately 37°C). No sample was found to have a long enough T_1 at lab temperature to mimic CSF at body temperature. Practically, deionized water may be the best choice as a CSF mimic because it is hard to reproducibly make extremely dilute agarose gels. One way to increase the T_1 time of deionized water at laboratory temperatures is to add deuterated water, which reduces the intermolecular relaxation sink. Although effective, this solution is not practical, as it increases cost and reduces signal intensity.[31] While individual $MnCl_2$ mimics for fat T_1 and T_2 can be made, fat lies outside of the T_1-T_2 space for $MnCl_2$, and thus, $MnCl_2$ is not recommended to mimic fat. We emphasize that the developed fat mimic formulation recommendations are for T_1

and T_2 values only, as they do not replicate fat's chemical shift. However, because chemical shift in absolute units (Hz) decreases with decreasing field strength, this is not a large concern for low magnetic fields.

Some $CuSO_4$ and $MnCl_2$ mimics had large differences between their measured T_1 and T_2 compared to the tissue T_1 and T_2 targets, which we attribute to inaccuracy within the fitted parameters for the mixing models themselves. For short T_1 and T_2, the $CuSO_4$ model predicted shorter T_1 and T_2 than measured in the mimics, which indicates low predictive capability in that region. This is because the training data for $CuSO_4$ measurements contain few samples in the short relaxation region. Improvements in the $CuSO_4$ mixing model could improve the accuracy of future $CuSO_4$ mimics. Additionally, $MnCl_2$ has higher relaxivity than the other salts (especially r_2), and thus, in the short relaxation region, the $MnCl_2$ mixing model exhibited a strong dependence of T_1 and T_2 on $MnCl_2$ concentration. Therefore, small inaccuracies in the model or in the concentration of $MnCl_2$ could result in large inaccuracies in the predicted T_1 and T_2 values. Improvements to both models could likely be made by including more samples for fitting.

The FFC T_1 data showed that while the salt and agarose curves generally do not overlap the tissue dispersion model curves, the salt and agarose concentrations can be chosen so that their curves intersect the dispersion curves at the field of their target mimic. The $GdCl_3$-EDTA curves most closely approximated the WM dispersion profile, and $GdCl_3$-EDTA is the best candidate for mimicking T_1 of WM and GM for a wide range of field strengths below 0.55 T based on the calculated percent errors of each formulation.

The mimic samples composed in this work are not meant to be perfect mimics for the calculated T_1 and T_2 times for each tissue and field. Rather, these mimics provide relaxation properties similar to tissue T_1 and T_2, using accessible materials.

4.3 | Other considerations

A challenge of achieving tissue-like samples is that the quantitative behavior of tissues is complex. For example, T_2 relaxation is generally multi-exponential. However, the more complex the tissue relaxation model is, the more difficult it is to find a mimic that satisfies all facets. Additionally, previous research found that multi-exponential T_2 measurements can vary substantially even within a tissue type.[34] For the purpose of this study, T_2 was modeled as a mono-exponential parameter. This simplified model makes consistency in measurements across many sites more feasible. Furthermore, this study focused on characterizing T_1 and T_2 times and did not consider other factors such as magnetization transfer, which has been shown to contribute to relaxation measurement variability.[35] Future improvements could be made to the study by modeling and measuring more complex material behavior.

When choosing the salt to use for sample creation and transportation, the safety of handling each material should be considered. According to safety data sheets from Millipore-Sigma, agarose and $GdCl_3$-EDTA are generally considered non-hazardous for shipping and handling. $CuSO_4$ has environmental hazards associated with it, and $MnCl_2$ and $NiCl_2$ are both considered toxic solids for shipping and handling; however, we did not find issues in shipping the samples made in this study due to the small concentrations used of each material. In general, these hazards should be considered when selecting sample materials.

4.4 | Conclusion

We created mixing models that can be used to find recipes for sample composition to target specific T_1 and T_2 relaxation times at 0.0065, 0.064, and 0.55 T. We created example sample mimics for five tissue types using the mixing models and evaluated their accuracy by measuring their relaxation properties at 0.0065, 0.0475, 0.05, 0.064, and 0.55 T. This work can help both qualitative and quantitative MRI method development for low-field systems and applications.

ACKNOWLEDGMENTS

This research was funded by the NIST (https://ror.org/05xpvk416) for K. V. J. (ORCID: 0000-0002-9097-3863), M. N. M. (ORCID: 0000-0002-4257-9589), S. E. O. (ORCID: 0000-0003-1098-1693), and K. E. K. (ORCID: 0000-0001-9070-5255). S. E. O. would like to acknowledge support from the NIST-PREP (Professional Research Experience Program), performed under the following financial assistance award 70NANB18H006 from the US Department of Commerce, National Institute of Standards and Technology. K. V. J. acknowledges research funding from the National Research Council Postdoctoral Fellowship. NIST acknowledges assistance from Hyperfine, Inc. (Guilford, CT) through a Cooperative Research and Development Agreement (CRADA). A.G.W. would like to acknowledge support from a Horizon 2020 ERC Advanced Grant (PASMAR 670629) and the Simon Stevin Prize from the Dutch Scientific Council (NWO). M. S. R. acknowledges the support of the Kiyomi and Ed Baird MGH Research Scholar award. M. S. R. is a founder and equity holder of Hyperfine, Inc. V. J. W. (ORCID 0000-0002-2718-6605) would like to acknowledge support from NIGMS NIH MOSAIC Pathway to Independence Award Grant K99GM140338-01 and the Intramural Research Program at NICHD. C. E. V., C. R. S., and W. A. G. would like to acknowledge support from the NIH grants R01 EB032709 and R01 EB030414. M. E. P. (ORCID 0000-0001-5474-8776) and R. P. T. (ORCID 0000-0001-6508-9315) are employees and equity holders of Hyperfine,

Inc. We acknowledge Dr. Gunjan Agarwal and Dr. Dana McTigue for IRB approval and assistance with tissue procurement. We acknowledge Dr. Samuel D Oberdick (ORCID: 0000-0003-4214-7492) for help with the ex vivo sample preparation.

CONFLICT OF INTEREST STATEMENT

This study was partially supported by a research grant from Hyperfine, Inc. Megan E. Poorman and Rui P. Teixeira are Hyperfine, Inc employees. Matthew S. Rosen is a founder and equity holder of Hyperfine, Inc.

DATA AVAILABILITY STATEMENT

The database of gathered measurements and code that support this study will be made openly available upon publication at these links: https://doi.org/10.18434/mds2-3063 and https://github.com/usnistgov/mri-tissue-mimics.

DISCLOSURES

Certain commercial equipment, instruments, or materials are identified in this paper in order to specify the experimental procedure adequately. Such identification is not intended to imply recommendation or endorsement by NIST, nor is it intended to imply that the materials or equipment identified are necessarily the best available for the purpose.

ORCID

Kalina V. Jordanova https://orcid.org/0000-0002-9097-3863
Ye Tian https://orcid.org/0000-0002-8559-4404
Charlotte R. Sappo https://orcid.org/0000-0002-7030-278X
Matthew S. Rosen https://orcid.org/0000-0002-7194-002X
Andrew G. Webb https://orcid.org/0000-0003-4045-9732
Kathryn E. Keenan https://orcid.org/0000-0001-9070-5255

REFERENCES

1. Marques JP, Simonis FFJ, Webb AG. Low-field MRI: an MR physics perspective. *J Magn Reson Imaging*. 2019;49(6):1528-1542. doi:10.1002/jmri.26637
2. Campbell-Washburn AE, Keenan KE, Hu P, et al. Low-field MRI: a report on the 2022 ISMRM workshop. *Magn Reson Med*. 2023;90(4):1682-1694. doi:10.1002/mrm.29743
3. Kimberly WT, Sorby-Adams AJ, Webb AG, et al. Brain imaging with portable low-field MRI. *Nat Rev Bioeng*. 2023;1(9):617-630. doi:10.1038/s44222-023-00086-w
4. Halse ME, Coy A, Dykstra R, et al. A practical and flexible implementation of 3D MRI in the Earth's magnetic field. *J Magn Reson*. 2006;182(1):75-83. doi:10.1016/j.jmr.2006.06.011
5. Sarracanie M, LaPierre CD, Salameh N, Waddington DEJ, Witzel T, Rosen MS. Low-cost high-performance MRI. *Sci Rep*. 2015;5(1):15177. doi:10.1038/srep15177
6. Cooley CZ, Stockmann JP, Armstrong BD, et al. Two-dimensional imaging in a lightweight portable MRI scanner without gradient coils. *Magn Reson Med*. 2015;73(2):872-883. doi:10.1002/mrm.25147
7. Lother S, Schiff SJ, Neuberger T, Jakob PM, Fidler F. Design of a mobile, homogeneous, and efficient electromagnet with a large field of view for neonatal low-field MRI. *Magma N Y N*. 2016;29(4):691-698. doi:10.1007/s10334-016-0525-8
8. Broche LM, Ross PJ, Davies GR, MacLeod MJ, Lurie DJ. A whole-body fast field-cycling scanner for clinical molecular imaging studies. *Sci Rep*. 2019;9(1):10402. doi:10.1038/s41598-019-46648-0
9. McDaniel PC, Cooley CZ, Stockmann JP, Wald LL. The MR cap: a single-sided MRI system designed for potential point-of-care limited field-of-view brain imaging. *Magn Reson Med*. 2019;82(5):1946-1960. doi:10.1002/mrm.27861
10. He Y, He W, Tan L, et al. Use of 2.1 MHz MRI scanner for brain imaging and its preliminary results in stroke. *J Magn Reson*. 2020;319:106829. doi:10.1016/j.jmr.2020.106829
11. Cooley CZ, McDaniel PC, Stockmann JP, et al. A portable scanner for magnetic resonance imaging of the brain. *Nat Biomed Eng*. 2021;5(3):229-239. doi:10.1038/s41551-020-00641-5
12. O'Reilly T, Teeuwisse WM, Gans D, Koolstra K, Webb AG. In vivo 3D brain and extremity MRI at 50 mT using a permanent magnet Halbach array. *Magn Reson Med*. 2021;85(1):495-505. doi:10.1002/mrm.28396
13. Liu Y, Leong ATL, Zhao Y, et al. A low-cost and shielding-free ultra-low-field brain MRI scanner. *Nat Commun*. 2021;12(1):7238. doi:10.1038/s41467-021-27317-1
14. Keenan KE, Gimbutas Z, Dienstfrey A, et al. Multi-site, multi-platform comparison of MRI T1 measurement using the system phantom. Lundberg P, ed. *PLOS One*. 2021;16(6):e0252966. doi:10.1371/journal.pone.0252966
15. Keenan KE, Ainslie M, Barker AJ, et al. Quantitative magnetic resonance imaging phantoms: a review and the need for a system phantom: quantitative MRI phantoms review. *Magn Reson Med*. 2018;79(1):48-61. doi:10.1002/mrm.26982
16. Mitchell MD, Kundel HL, Axel L, Joseph PM. Agarose as a tissue equivalent phantom material for NMR imaging. *Magn Reson Imaging*. 1986;4(3):263-266. doi:10.1016/0730-725X(86)91068-4
17. Walker P, Lerski RA, Mathur-De Vré R, Binet J, Yane F. VI. Preparation of agarose gels as reference substances for NMR relaxation time measurement. *Magn Reson Imaging*. 1988;6(2):215-222. doi:10.1016/0730-725X(88)90452-3

18. Christoffersson JO, Olsson LE, Sjöberg S. Nickel-doped agarose gel phantoms in MR imaging. *Acta Rudiologica*. 1991;32(5):426-431. doi:10.1177/028418519103200519
19. Martin MN, Jordanova KV, Kos AB, Russek SE, Keenan KE, Stupic KF. Relaxation measurements of an MRI system phantom at low magnetic field strengths. *Magn Reson Mater Phys Biol*. 2023;20(3):477-485. doi:10.1007/s10334-023-01086-y
20. Howe FA. Relaxation times in paramagnetically doped agarose gels as a function of temperature and ion concentration. *Magn Reson Imaging*. 1988;6(3):263-270. doi:10.1016/0730-725X(88)90400-6
21. Hattori K, Ikemoto Y, Takao W, et al. Development of MRI phantom equivalent to human tissues for 3.0-T MRI. *Med Phys*. 2013;40(3):032303. doi:10.1118/1.4790023
22. Gopalan K, Tamir JI, Arias AC, Lustig M. Quantitative anatomy mimicking slice phantoms. *Magn Reson Med*. 2021;86(2):1159-1166. doi:10.1002/mrm.28740
23. DeVience SJ, Rosen MS. Homonuclear J-coupling spectroscopy using J-synchronized echo detection. *J Magn Reson*. 2022;341:107244. doi:10.1016/j.jmr.2022.107244
24. O'Reilly T, Teeuwisse WM, Webb AG. Three-dimensional MRI in a homogenous 27 cm diameter bore Halbach array magnet. *J Magn Reson*. 2019;307:106578. doi:10.1016/j.jmr.2019.106578
25. Kraft M, Ryger S, Berman BP, et al. Towards a barrier-free anthropomorphic brain phantom for quantitative magnetic resonance imaging: design, first construction attempt, and challenges. *PLoS ONE*. 2023;18(7):e0285432. doi:10.1371/journal.pone.0285432
26. Singhrao K, Fu J, Wu HH, et al. A novel anthropomorphic multimodality phantom for MRI-based radiotherapy quality assurance testing. *Med Phys*. 2020;47(4):1443-1451. doi:10.1002/mp.14027
27. Deene YD, Wheatley M, Greig T, Hayes D, Ryder W, Loh H. A multi-modality medical imaging head and neck phantom: part 1. Design and fabrication. *Phys Medica Eur J Med Phys*. 2022;96:166-178. doi:10.1016/j.ejmp.2022.02.010
28. Wood S, Krishnamurthy N, Santini T, et al. Design and fabrication of a realistic anthropomorphic heterogeneous head phantom for MR purposes. *PLoS ONE*. 2017;12(8):e0183168. doi:10.1371/journal.pone.0183168
29. Crasto N, Kirubarajan A, Sussman D. Anthropomorphic brain phantoms for use in MRI systems: a systematic review. *Magn Reson Mater Phys Biol Med*. 2022;35(2):277-289. doi:10.1007/s10334-021-00953-w
30. Winslow JF, Hyer DE, Fisher RF, Tien CJ, Hintenlang DE. Construction of anthropomorphic phantoms for use in dosimetry studies. *J Appl Clin Med Phys*. 2009;10(3):195-204. doi:10.1120/jacmp.v10i3.2986
31. Stupic KF, Ainslie M, Boss MA, et al. A standard system phantom for magnetic resonance imaging. *Magn Reson Med*. 2021;86(3):1194-1211. doi:10.1002/mrm.28779
32. Nelson TR, Tung SM. Temperature dependence of proton relaxation times in vitro. *Magn Reson Imaging*. 1987;5(3):189-199. doi:10.1016/0730-725x(87)90020-8
33. Statton BK, Smith J, Finnegan ME, Koerzdoerfer G, Quest RA, Grech-Sollars M. Temperature dependence, accuracy, and repeatability of T1 and T2 relaxation times for the ISMRM/NIST system phantom measured using MR fingerprinting. *Magn Reson Med*. 2022;87(3):1446-1460. doi:10.1002/mrm.29065
34. Dula AN, Gochberg DF, Valentine HL, Valentine WM, Does MD. Multi-exponential T2, magnetization transfer and quantitative histology in white matter tracts of rat spinal cord. *Magn Reson Med off J Soc Magn Reson Med Soc Magn Reson Med*. 2010;63(4):902-909. doi:10.1002/mrm.22267
35. Teixeira RPAG, Neji R, Wood TC, Baburamani AA, Malik SJ, Hajnal JV. Controlled saturation magnetization transfer for reproducible multivendor variable flip angle T1 and T2 mapping. *Magn Reson Med*. 2020;84(1):221-236. doi:10.1002/mrm.28109

SUPPORTING INFORMATION

Additional supporting information can be found online in the Supporting Information section at the end of this article.

How to cite this article: Jordanova KV, Fraenza CC, Martin MN, et al. Paramagnetic salt and agarose recipes for phantoms with desired T1 and T2 values for low-field MRI. *NMR in Biomedicine*. 2024;e5281. doi:10.1002/nbm.5281